J Mater Sci (2011) 46:243–253
DOI 10.1007/s10853-010-4966-6

The effect of high temperature heat treatment on the structure and properties of anodic aluminum oxide

M. Kylan McQuaig Jr. · Alejandro Toro · William Van Geertruyden · Wojciech Z. Misiolek

Received: 26 May 2010 / Accepted: 29 September 2010 / Published online: 14 October 2010
© Springer Science+Business Media, LLC 2010

Abstract Nanoporous anodic aluminum oxide (AAO) membranes can be fabricated with highly controllable thickness and porosity, making them ideal for filtration applications. Use of these membranes is currently limited largely due to their size and overall fragility. The objective of this research was to improve mechanical properties of AAO membranes through use of high temperature heat treatment to induce phase transformations in the material. A repeatable two-step anodization process was developed for consistent sample fabrication and heat treatments were performed at 900 °C and 1200 °C in air. The pore morphology and phase composition of the as-anodized and heat-treated membranes were then observed using scanning electron microscopy (SEM) and transmission electron microscopy (TEM). Microhardness testing was utilized to evaluate the mechanical behavior of the membranes before and after heat treatment. As-anodized AAO membranes were determined to be amorphous, and membranes heat-treated to 900 °C and 1200 °C were transformed to crystalline phases while retaining their original porous structure. Heat treatment to 900 °C resulted in formation of the γ-alumina transition phase in the skeleton regions of the membrane and nanocrystalline regions of α-alumina throughout the structure, while heat treatment to 1200 °C completely transformed the material to the stable α-alumina structure. The microhardness testing showed an increase in hardness from 2.5 $\pm$ 0.4 GPa to 4.7 $\pm$ 1.0 GPa in the transformation from amorphous to α-alumina.

M. K. McQuaig Jr. · W. Z. Misiolek
Institute for Metal Forming, Lehigh University, Bethlehem, PA, USA

W. Van Geertruyden
EMV Technologies, LLC, Bethlehem, PA, USA

A. Toro (✉)
Tribology and Surfaces Group, National University of Colombia, Medellin, Colombia
e-mail: aotoro@unal.edu.co

Introduction

Anodic aluminum oxide (AAO) has been utilized since the early 1900s as a protective coating and for coloring purposes on aluminum and its alloys. In 1953, Keller et al. [1] proposed a model for porous AAO based on an array of ordered nanopores, with each individual pore contained within a hexagonal cell. In 1995, Masuda and Fukuda [2] discovered the self-ordering mechanism of pores in AAO through the use of a two-step anodization procedure. The fabrication of AAO membranes with self-organized pore structures has been well-reported and utilized as templates for a variety of nanostructures [3–6].

In 1981, Thompson and Wood [7] reported that the AAO microstructure can be separated into two regions: a relatively pure alumina region (inner layer), consisting entirely of Al_2O_3, and an acid anion-contaminated region (outer layer), resulting from incorporation of anions into the alumina structure during anodization. Vrublevsky et al. [8] have reported a similar structure, with 90% of the oxide comprised of the outer layer and 10% comprised of the inner layer. These regions were investigated and verified by Ko et al. [9] using a scanning transmission electron microscope (STEM).

Recently, the phases present within the AAO structure have been of interest to those hoping to use AAO membranes in applications requiring mechanical strength. Extensive X-ray diffraction (XRD) and transmission electron microscopy (TEM) work has been performed to

determine that the as-anodized alumina is amorphous, and that heat treatment of amorphous AAO at high temperatures will lead to changes in crystal structure [9–13]. In addition to possible improvements to mechanical properties, it has been reported that heat treatment of amorphous membranes at high temperature may improve thermal stability and resistance to chemical attack [14].

The thermodynamically stable phase of alumina is α-Al_2O_3 (corundum). Aluminum oxide also exists in a wide array of metastable polymorphs, sometimes referred to as "transition aluminas." These metastable structures fall under one of two categories: face-centered cubic (FCC) or hexagonal close-packed (HCP) in terms of the oxygen anion sublattice. FCC aluminas include γ, η, θ, θ', θ'', δ, and λ types, while HCP aluminas include α, κ, and χ types. As reported by Levin and Brandon [15], alumina polymorphs are based on FCC or HCP packing of oxygen in the sublattice, with aluminum in the tetrahedrally and octahedrally coordinated interstitial sites.

In order to understand the transformation of amorphous AAO into α-Al_2O_3, it is important to examine the exact transformation sequence including intermediate phases. Levin and Brandon [15] determined many common transformation routes to the stable α-Al_2O_3 phase, including the transformation route from an AAO precursor as follows:

$$\text{Amorphous (anodic film)} \rightarrow \gamma \rightarrow \delta \rightarrow \theta \rightarrow \alpha - Al_2O_3$$

Similar transformation sequences were reported other researchers from amorphous aluminum oxides fabricated using methods other than anodization [16, 17]. It is reported in literature that the complete transformation from amorphous alumina to α-Al_2O_3 will occur between 1000 °C and 1200 °C with heat treatments of only 1 h [11].

In contrast, several authors reported that heat treatment at temperatures equal to or greater than 1200 °C was necessary to complete the transformation of amorphous AAO to α-alumina. Differential scanning calorimetry (DSC) has been used to measure the heat flow in the sample during heat treatment to determine the exact temperatures at which phase transformations would occur. In addition, thermogravimetric analysis (TGA) has been used to measure the weight loss of the material versus temperature. The TGA results, coupled with mass spectrometry, have allowed researchers to determine the amount of decomposition and removal of chemical species from the sample as temperature is increased [18].

Mata-Zamora and Saniger [19] observed transition phase formation at 900 °C and a transformation to α-alumina just above 1200 °C using DSC analysis. They performed both DSC and TGA analysis on AAO membranes fabricated in sulfuric acid, oxalic acid, and phosphoric acid electrolytes. In general, it was found that the electrolyte used during anodization has a strong effect on transformation temperatures during heat treatment. It has been reported that dehydration of the AAO membranes occurs up to 400 °C, dehydroxylation occurs between 400 °C and 700 °C, and incorporated species from the electrolyte decompose at high temperatures before the final transformation to α-alumina [14]. The variation in chemistry of membranes fabricated in each electrolyte and the corresponding decomposition during heat treatment is likely the cause in the large difference in transformation temperature to α-alumina [19–21].

Experimental procedure

Fabrication of AAO membranes

Aluminum sheets (99.99% metals bias) were used as anodes and graphite sheets were used as cathodes in the fabrication of AAO membranes. Aluminum and graphite sheets were cut into sections measuring 3 cm × 4 cm for use in the anodization process. The aluminum sheets were first electropolished for 45 s at a constant current of 45 A in a solution consisting of 235 mL orthophosphoric acid, 190 mL 95 vol% ethanol, and 100 mL deionized water in order to improve surface quality of the substrate. An acrylic coating was applied to one side of the aluminum and first anodization was performed for 2 h at a constant voltage of 40 V in a 2.7 wt% oxalic acid solution. The initial oxide was removed in a solution composed of 4 wt% chromic acid and 8 wt% orthophosphoric acid at a ratio of 1:1, after an exposure time of 1 h at 60 °C. The desired membrane thickness (greater than 50 μ) was achieved after a 20-h second anodization, using the same electrolyte and applied voltage. During both anodization steps, the electrolyte temperature was maintained between 0 and 5 °C using an ice water bath. Following second anodization, the aluminum substrate was etched away in a solution composed of 0.1 M copper chloride and 10 vol% hydrochloric acid at a ratio of 4:1 for 8 h, and the barrier layer was removed using an 0.1 M orthophosphoric acid solution for 1 h. All steps were performed at room temperature unless otherwise noted.

Heat treatments

In order to determine the exact temperatures at which crystalline transformations would occur during heat treatment, DSC analysis was performed on an as-anodized and a commercial AAO sample using a Netzsch STA 409. The commercial samples were circular Whatman membranes with a nominal pore size of 100 nm, a diameter of 13 mm, and a membrane thickness of 60 μ. Using TGA, the mass loss of the material during heat treatment was also

monitored. Using expected transformation temperatures for the membranes obtained from DSC tests, heat treatment was then performed in air in a Thermo Scientific tube furnace. Peak heat treatment temperatures of 900 and 1200 °C were chosen slightly higher than the temperatures in the DSC analysis corresponding to expected phase transformation. Samples were held at peak temperature for 1 h, and an extremely low constant heating and cooling rate of 1 °C/min was chosen to prevent thermal cracking of the material.

Microstructural characterization

Microstructural characterization and analysis was performed using a Hitachi 4300 FEG SEM and a JEOL 2000FX TEM. The specimens were observed in the SEM before and after heat treatment in order to analyze changes in size and morphology of the pores. Samples were prepared for the TEM using a focused ion beam (FIB) technique on a FEI Strata DB 235, by thinning a small portion of the membrane to approximately 200 nm. Diffraction patterns of as-anodized and heat-treated samples were taken and indexed in order to determine the phases present within the samples. JCPDS-ICDD cards N. 10-0173, 10-0425, 35-0121 and 16-0394 were used for α, γ, θ, and δ phases, respectively.

Mechanical testing

Microhardness testing was performed using a LECO M400FT hardness tester and a Vickers diamond pyramid indenter. Several loads were used, but it was found that a 300 g load provided an optimal indentation in the material without cracking the samples. The Vickers Hardness was then calculated using the area of the resulting indentation in the sample and the applied load. Any indentations resulting in a large amount of cracking within the membrane were discarded as the corresponding hardness value was not considered valid. Microhardness testing was performed in 10 locations on two as-anodized samples and the average hardness value of the as-anodized samples was calculated. This was repeated for two samples heat-treated at 1200 °C to determine the average hardness of the heat-treated samples.

Results and discussion

Pore morphology

A comparison of high magnification SEM images taken before and after heat treatment to 1200 °C is shown in Fig. 1. A regular pore structure can be observed both before and after heat treatment of the membranes. There is a loss of the overall round shape of the pores, as the pore walls appear to have become slightly deformed by the heat treatment. The circularity of the pores, defined as $C = 4\pi A/P^2$, where P is the perimeter and A is the area of the pore [22], was used to quantify this change and the results are shown in Table 1.

The results from Table 1 show that, as a consequence of heat treatment performed at 1200 °C, an increase in average pore size of 15.3% and a loss of circularity of 6.7% were observed, while the number of pores per unit area dropped from 94 to 82 pores/μm^2.

A change in the overall pore structure of AAO membranes is expected during heat treatment to high temperature, largely due to the increase in density that accompanies the phase transformation from amorphous to crystalline α-alumina. Because there is an increase in density during phase transformation, accompanied simultaneously by a reduction in mass due to the dehydration, dehydroxylation, and loss of anions, a substantial decrease in the overall volume of the membrane and consequently in the effective pore density is to be expected. It has been reported in literature that heat treatment will result in cracking perpendicular to the pore channels [20]. In this research, the straight-channel pores remained reasonably unaffected and

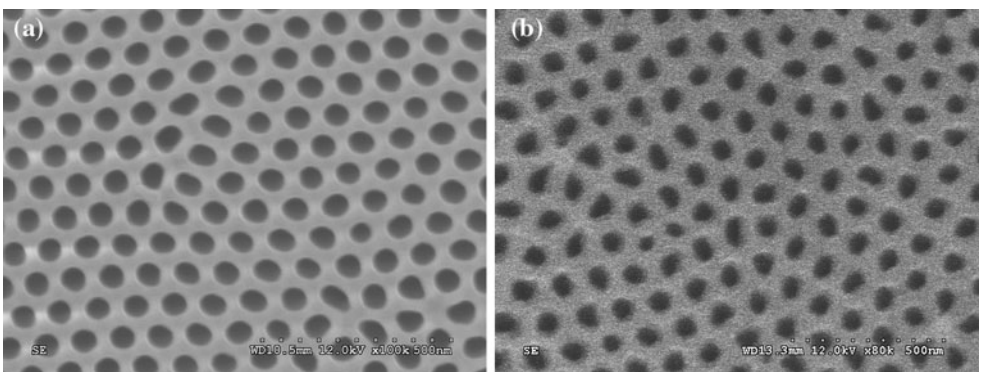

Fig. 1 High magnification SEM image of AAO pore structure before heat treatment (**a**) and after heat treatment to 1200 °C (**b**)

Table 1 Changes in pore morphology due to heat treatment at 1200 °C

	$C = 4\pi A/P^2$	Average pore size (nm)[a]	PD (pores/μm^2)[b]
Before heat treatment	0.89 ± 0.04	75.5 ± 9.2	94
After heat treatment	0.83 ± 0.05	87.1 ± 14.0	82

[a] Mean value of maximum feret measurements

[b] *PD* number of pores per unit area

only minor morphological changes were observed after heat treatment as can be seen in Table 1, which is in agreement with the results from Kirchner et al. [18] and Fernandez-Romero et al. [23]. Accordingly, the structure can be considered suitable for manufacturing diverse biomedical devices such as hemodialysis membranes, where an uneven distribution of pore size and shape can cause protein leaking problems and adsorption of small molecules inside the membrane [24].

Phase transformations

Figure 2 shows both heat flow and mass% versus temperature for a fabricated AAO membrane before heat treatment. Early features of both curves can be attributed largely to dehydration and dehydroxylation of the membrane. As reported previously, dehydration will occur up to 400 °C and dehydroxylation will occur up to 700 °C [14].

A large exothermic peak was observed in the DSC curve at approximately 860 °C, corresponding to the expected transformation temperature of amorphous alumina to γ-alumina. The formation of this transition phase is in good agreement with other DSC results the literature, found to form between 850 and 900 °C for the same electrolyte and similar heating rates [19, 20]. According to DSC results in literature, the exothermic peak corresponding to a transition to α-alumina should have been present between 1000 and 1200 °C [14, 19, 20]. While such a well-defined peak was not observed in the sample, evidence of internal transformations occurring in the material after γ-alumina formation can be recognized in Fig. 2. In particular, it is noted that a reduction of specific volume accounts for a compensation of thermal expansion up to approximately 1000 °C, where the slope of the DSC curve becomes stable and the microstructure is likely composed mostly of the α-alumina phase. These results suggest that the α-alumina structure becomes stable at temperatures far below 1200 °C.

The TGA curve in Fig. 2 shows a steady loss of mass up to approximately 800 °C, which has been credited to loss of H_2O and OH-species during the dehydration and dehyroxilation processes, respectively. A sharp drop of mass is seen at the same point as the large exothermic peak seen in the DSC curve at 860 °C. At this point, the transition of amorphous AAO to γ-alumina is expected to begin, as well as the thermal decomposition of the incorporated anions within the alumina structure. For membranes fabricated with oxalic acid, this compound is likely CO_2. Further testing would be needed to determine the exact composition of the decomposing species, but the large drop in mass following the transition to γ-alumina is supported by the literature [19].

The DSC and TGA curves for the commercial sample can be seen in Fig. 3. While the early peaks corresponding to dehydration and dehydroxylation are not as pronounced in DSC results of the commercial sample when compared to the results shown in Fig. 2, the exothermic peaks corresponding to γ-alumina phase formation are in good agreement in both DSC curves. The exact processing

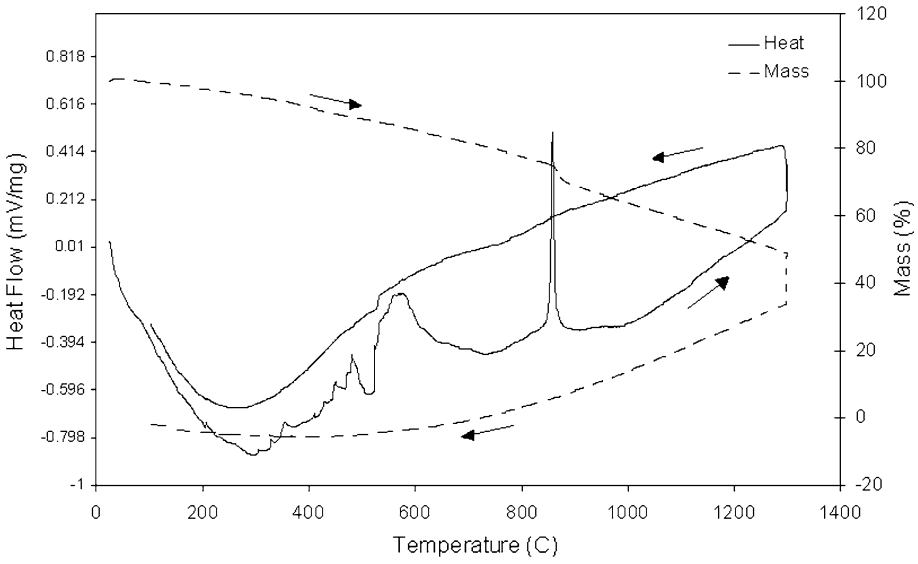

Fig. 2 DSC and TGA curves for an oxalic acid-fabricated sample

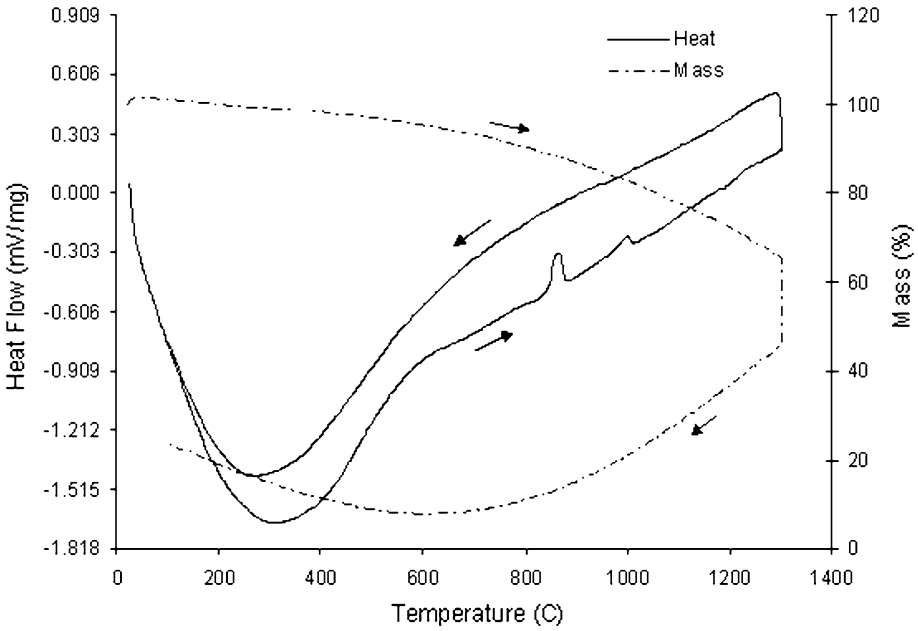

Fig. 3 DSC and TGA curves for a commercial membrane

parameters of Whatman membranes are unknown, but it is possible that the commercial membranes were put through a low temperature heat treatment following fabrication to promote dehydration and dehydroxylation before their sale. The DSC results of the commercial sample display a more prominent exothermic peak just below 1000 °C, where the transformation to α-alumina is expected to occur, but both samples appear to be completely stable above 1100 °C. The actual phases observed after heat treating at 900 °C and 1200 °C will be described in detail in the following.

Microstructural characterization

Before any heat treatments were performed, TEM characterization of the as-anodized samples was done. A bright-field TEM image of the pore cross-section and the diffuse diffraction rings from the as-anodized sample are shown in Fig. 4. The image in Fig. 4b supports the well-known belief that AAO has an amorphous structure. Straight-channel pores can be seen and their amorphous structure will be used in comparison to the heat-treated samples at 900 and 1200 °C.

As discussed earlier, AAO consists of an anion-incorporated region surrounding each of the pores and a pure alumina [7]. Figure 5 shows a TEM image of a commercial membrane heat-treated to 900 °C. As shown in the image, the pure alumina skeleton is the first region to become crystalline. A higher magnification TEM image of the same sample is shown in Fig. 6 with the anion-incorporated region (A) and pure alumina skeleton (B) labeled. The

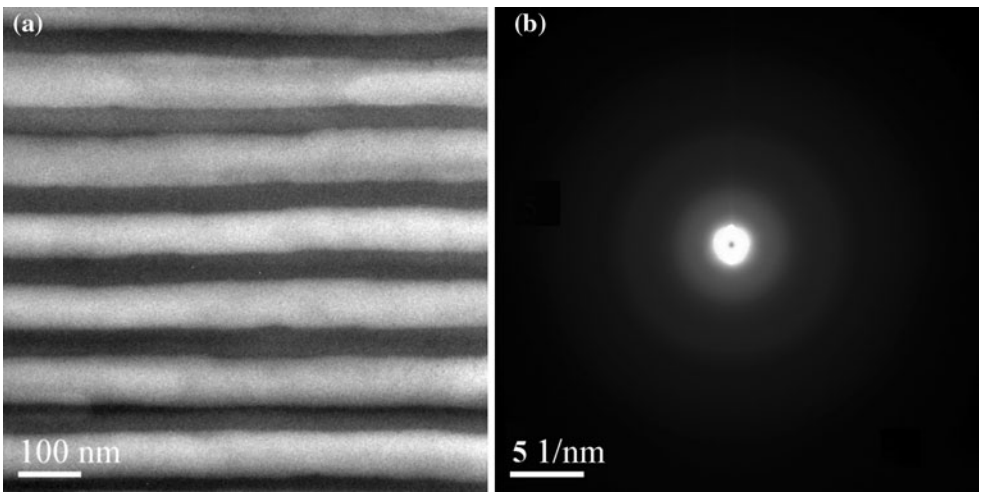

Fig. 4 Bright-field TEM image of as-anodized AAO sample (**a**) and corresponding diffuse diffraction rings (**b**)

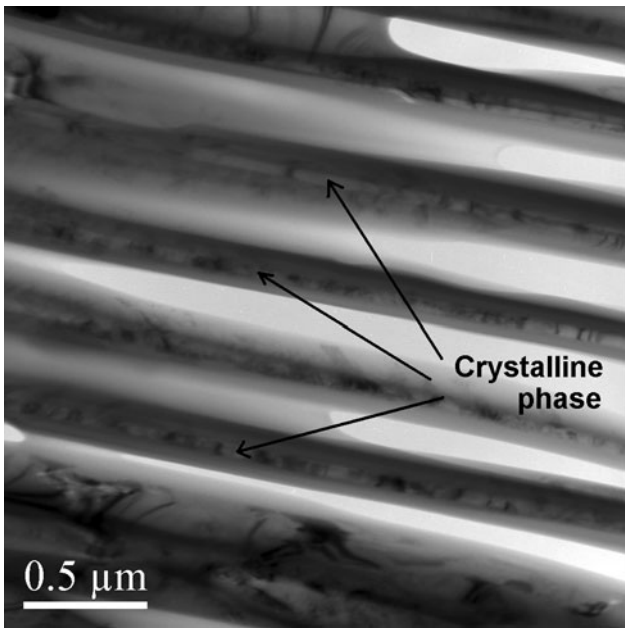

Fig. 5 Bright-field TEM image of commercial membrane heat-treated to 900 °C with important features labeled

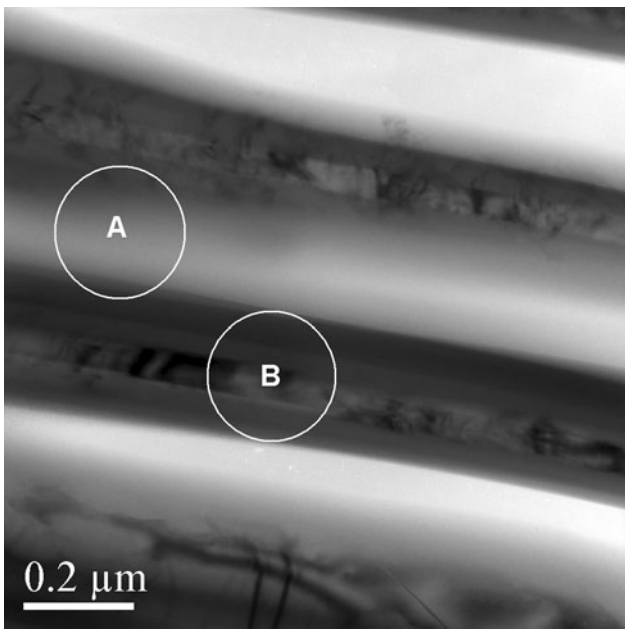

Fig. 6 Bright-field TEM image of commercial membrane heat-treated to 900 °C with amorphous anion-incorporated region (**a**) and crystallized pure alumina region (**b**) labeled

diffraction patterns corresponding to these two regions within the commercial membrane are then shown in Fig. 7. As seen in this figure, after heat treatment at 900 °C, the anion-incorporated region still shows a diffuse diffraction pattern corresponding to an amorphous structure. Meanwhile, the pure alumina region has crystallized and shows a spot pattern corresponding to crystalline γ-alumina.

As suggested in the literature, the difference in microstructure can be explained by the difference in chemical composition across the walls of the membrane resulting from the incorporation of anions during anodization. While the pure alumina region of the AAO has undergone a crystalline transformation after heat treatment at 900 °C, the anion-incorporated region remains amorphous. Before the crystalline transformation occurs in this region, it is possible that decomposition of the incorporated species must occur first.

The samples fabricated from the oxalic acid electrolyte and heat-treated at 900 °C showed similar features to the commercial membranes in terms of the regions observed in the samples. Both samples were found to be completely amorphous before heat treatment and exhibited a pure alumina skeleton region with a crystalline γ phase after heat treatment at 900 °C. The skeleton regions in the commercial membranes were approximately 50 nm in width, while these regions in the oxalic acid membranes were less defined and were found to be only 25 nm wide. The commercial samples showed a more developed crystalline structure within the skeleton regions, displaying well-developed shear bands within the crystals and high order diffraction spots.

Figure 8 shows one of the membranes fabricated in oxalic acid and the corresponding diffraction pattern. The thin skeleton region can be observed in Fig. 8a, consisting primarily of γ-alumina. The ring diffraction pattern obtained from a region of the sample including both the skeleton and the anion-incorporated areas shows that the γ phase is present in the material as expected, but the outer rings in the pattern also show a contribution from the α phase. None of the rings matched the expected positions corresponding to the interplanar spacings in θ and δ transition aluminas. This nanocrystalline α phase, seen in the TEM bright-field image as small dark regions, was found to form outside of the γ crystalline strips in the amorphous anion-incorporated region. The presence of the α phase is unexpected at 900 °C and contradicts the transition temperatures reported by previous research [15, 18, 25].

A higher magnification TEM image of the sample is shown in Fig. 9a with an area of interest circled for phase identification. Limitations of the spatial resolution in the instrumentation made direct identification of the nanocrystalline regions difficult, so identification of the phase contribution in the remaining area was performed. The area of interest encompasses as little of the nanocrystalline phase as possible, in order to ensure that the remainder of the sample consisted primarily of the γ phase as expected with little or no contribution from the α phase. The indexed spot pattern from this area can be seen in Fig. 9b, identifying the crystalline phase in the skeleton region as γ-alumina.

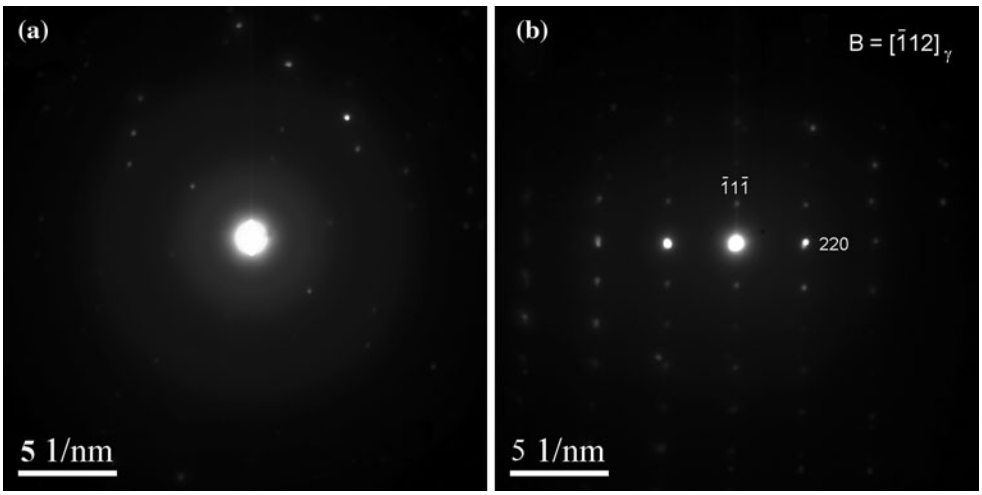

Fig. 7 Diffraction patterns from the anion-incorporated region (**a**) and pure alumina region (**b**) in Fig. 6

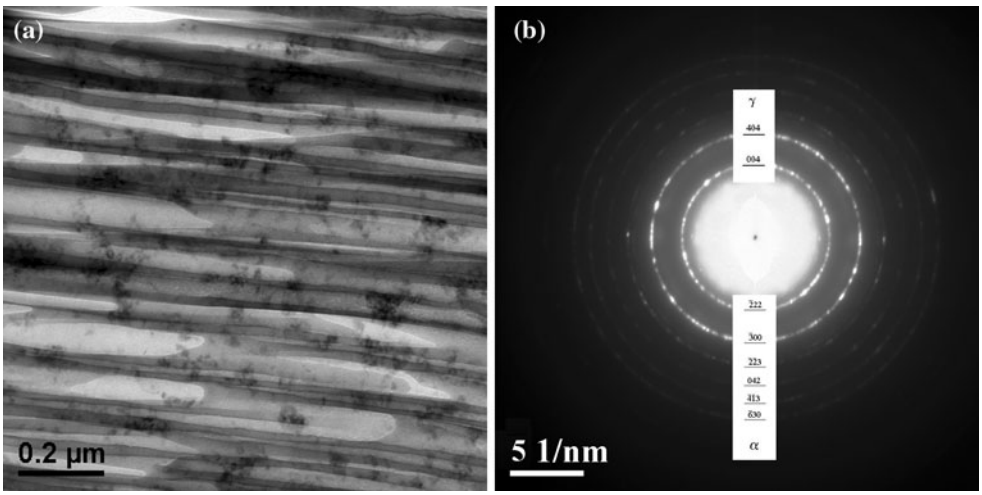

Fig. 8 Bright-field TEM image of a sample heat-treated to 900 °C (**a**) and corresponding ring pattern, showing contributions from both γ- and α-alumina phases (**b**)

The diffraction rings in Fig. 8b show that α-alumina is present in samples heat-treated to just 900 °C. The low intensities and complete absence of several of the α-alumina rings may suggest that the first α-alumina grains may form with preferential orientations. It is possible to speculate also that the phase transition sequence as accepted in the literature [15] may only apply to the pure alumina skeleton region.

The transition from amorphous AAO to γ-alumina is expected between approximately 850 and 900 °C, while the final transition to α-alumina is expected between 1000 and 1200 °C. The skeleton region appears to follow the expected transition sequence, but the anion-incorporated region appears to show a transformation to α-alumina at a much lower temperature. Meanwhile, the anion-incorporated region remains amorphous after heat treatment to 900 °C with nucleation of nanocrystalline regions of α-alumina. Further work needs to be performed to fully understand what mechanisms drive the unanticipated nucleation and growth of α phase below 1000 °C.

Figure 10a shows a TEM image of a sample fabricated in oxalic acid and heat-treated to 1200 °C. The samples heat-treated to 1200 °C showed a higher degree of crystallinity and stability than the samples heat-treated to 900 °C. After this high temperature heat-treatment, the samples consisted completely of the α phase. As seen in the figure, there was some coalescence of the nanocrystalline α grains.

Figure 10b shows the ring diffraction pattern taken from one of these samples. The diffraction pattern shows the presence of the α phase exclusively in the sample, as the γ phase from the skeleton regions as well as the amorphous material in the anion-incorporated region transformed completely to α-alumina.

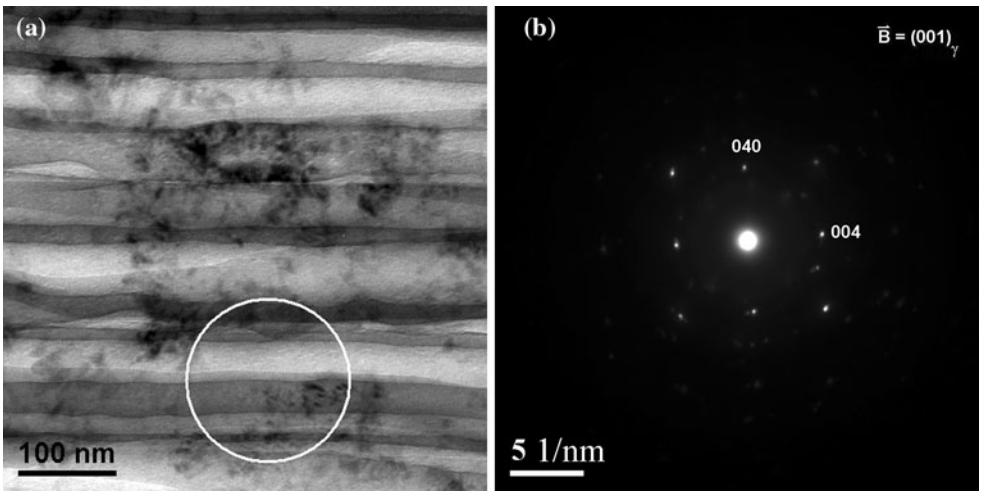

Fig. 9 Higher magnification bright-field TEM image from the sample heat-treated to 900 °C with the area of interest *circled* (**a**) and spot pattern from area corresponding to γ-alumina phase (**b**)

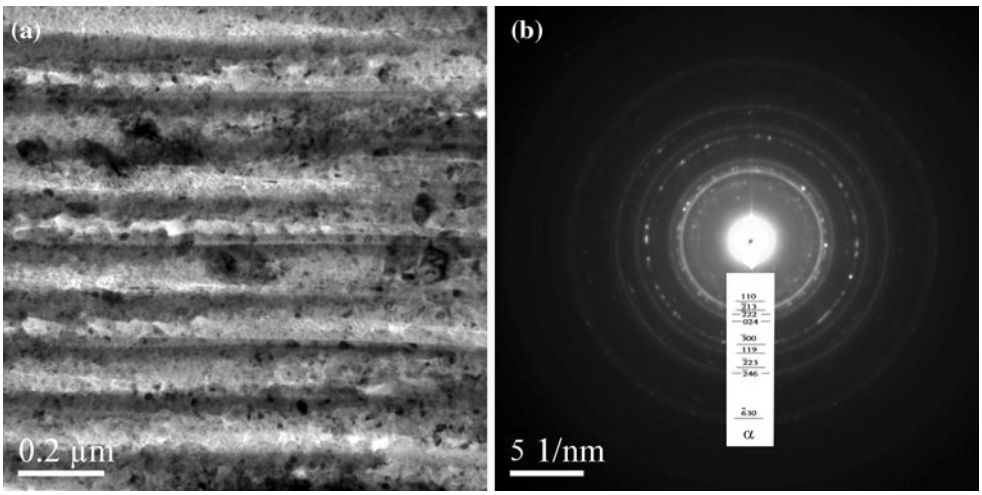

Fig. 10 Bright-field TEM image of a sample heat-treated to 1200 °C (**a**) and corresponding ring pattern, showing contribution from α-alumina phase only (**b**)

The increased number of rings in the diffraction pattern in Fig. 10b show that the α crystals became more randomly oriented throughout the sample, though some differences in relative ring intensities when compared to the expected ring pattern could still provide evidence of one or more favorable orientations during α formation. For instance, the (300) ring in Fig. 10b is expected to have the highest intensity of the pattern, but the intensities of the (213) and (222) rings are comparable or even higher in the observed ring pattern. Also, the (300) ring shows a high amount of discontinuity. This provides further evidence of favorable orientations during α-alumina growth.

A high magnification TEM image of a large α-alumina crystal is shown in Fig. 11a, along with the corresponding spot pattern in Fig. 11b. The spot pattern has clearly been identified as α phase, supporting the theory of nanocrystalline α crystal nucleation and growth with increasing temperature.

Mechanical properties

A microindentation such as the one in the Fig. 12a was accepted after observation in the light optical microscopes and the corresponding hardness value was recorded, because no cracking was observed in the area of the indentation. A high magnification SEM image of this indentation can be seen in Fig. 12b, showing the presence of a microcrack approximately 1.5 μm in length that was indistinguishable using light optical microscopy alone. Features such as microcracking within the microindentations could have an effect on the final measured hardness value.

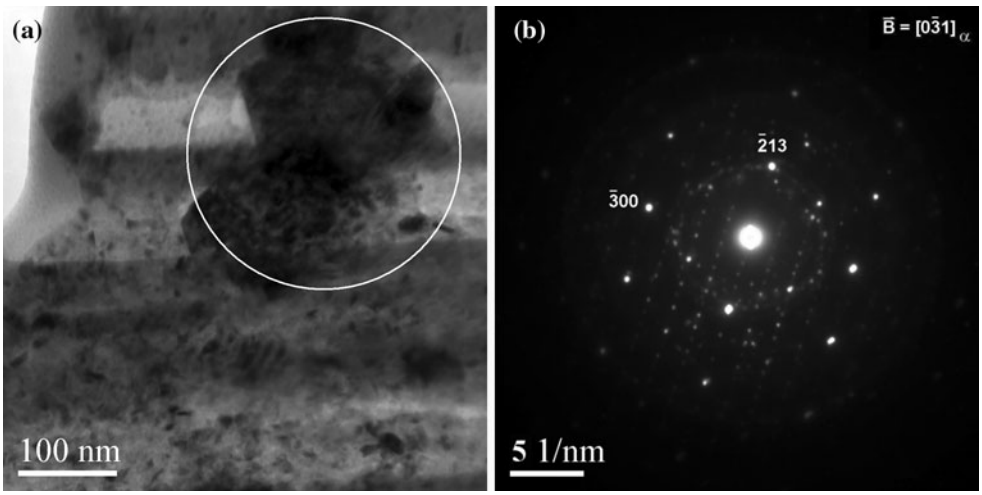

Fig. 11 Higher magnification TEM image from the sample heat-treated to 1200 °C with enlarged nanocrystal *circled* (**a**) and spot pattern from nanocrystal corresponding to α-alumina phase (**b**)

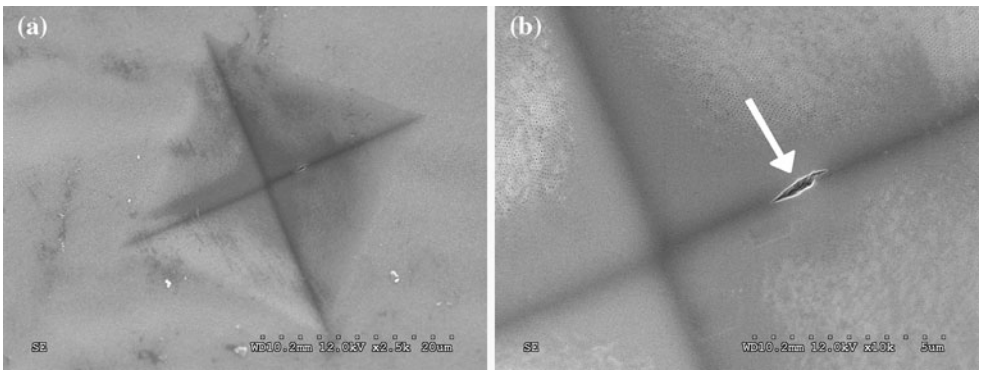

Fig. 12 SEM image of a microindentation (**a**) displaying microcrack formation (**b**) in an amorphous AAO membrane

Table 2 Microhardness data for 20 areas in amorphous and α-alumina membranes

	As-anodized (amorphous)		Heat-treated to 1200 °C (α-alumina)	
	Hardness (HV_{300gf})	Hardness (GPa)	Hardness (HV_{300gf})	Hardness (GPa)
Average	252.2	2.5	474.7	4.7
Standard deviation	42.8	0.4	103.0	1.0

The microhardness values observed in amorphous and α-alumina AAO membranes are presented in Table 2. While a substantial standard deviation was found using the microhardness testing technique, it is important to note a significant increase in hardness from the amorphous to the crystalline AAO membranes. The average hardness in the measured samples increases by nearly a factor of two through heat treatment of AAO alone. While it was difficult to achieve high precision within these experiments, the overall trend shows a definite increase in hardness after heat treatment to 1200 °C and resulting crystalline transformation. The measured hardness of the samples treated at 1200 °C (4.7 ± 1 GPa) is significantly lower than the values found in literature for pure, well crystalline corundum or sapphire, which are usually in the range between 20 and 25 GPa [26, 27]. This difference is mainly attributed to the porous structure, which is responsible for the unique mechanical response of the membranes as discussed below.

One potential source of error associated with microhardness testing of AAO can be explained through the microcracking seen in Fig. 12b. Cracking within a material will affect the size of the microindentation by reducing the amount of deformation in response to the applied load. In turn, the length of the average diagonal will be lower in the

indentation and the apparent hardness of the material will be slightly higher. In addition, the overall porosity of the material and defect presence following the anodization procedure may result in variation in the measured microhardness data.

Considering that alumina is a ceramic material, the actual mechanism of deformation within the material during microindentation comes into question. A high magnification SEM image of an indentation in an amorphous membrane is shown in Fig. 13, in which pore crushing is evident as the mechanism causing the permanent indentation in the material. The corner of the indentation, seen in Fig. 13, is surrounded by the normal pore structure, while the pores appear deformed within the indentation due to overall collapse of the porous structure. The same mechanism is observed in Fig. 14a in a crystalline α-alumina membrane. A SEM image taken at even higher magnification presented in Fig. 14b shows not only crushing of the pores under the force of the indenter but nanocrack initiation between the pores as well.

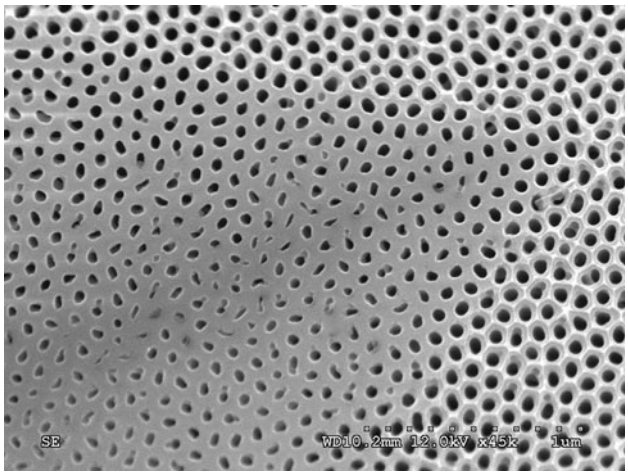

Fig. 13 High magnification SEM image of the corner of a microindentation exhibiting pore crushing in an amorphous membrane

Rather than through pure material plasticity, the overall structure of both amorphous and crystalline nanoporous AAO membranes is permanently deformed by the indenter through pore collapse and crack initiation. These mechanisms of apparent deformation are established and have also been observed by Gall et al. [11] and Xia et al. [12]. Ng et al. [28] used focused ion beam milling in order to observe the cross-sections of the microindentations in great detail. It was observed that while the underlying porous structure remains intact, crack formation perpendicular to the pore columns under the indenter load causes crushing of the porous structure towards the indentation. Microhardness values between 3.5 and 8 GPa for amorphous AAO membranes have commonly been reported in the literature [29], but because of the unusual deformation mechanisms and the nanoporous structure of the material, there is some error inherent in the process.

Conclusions

The effect of high temperature heat treatment on the pore structure, phase composition, and mechanical properties of AAO membranes was investigated in this research. Amorphous membranes were fabricated using a repeatable two-step anodization process and an oxalic acid electrolyte. High temperature heat treatment at 900 °C resulted in a transformation to the metastable γ-alumina phase with nanocrystalline regions of α-alumina, while heat treatment to 1200 °C resulted in a complete transformation to the thermodynamically stable α-alumina phase. Based on observations and the data acquired, the following conclusions were drawn:

- AAO membranes heat-treated at high temperature maintain their overall porous structure and straight-channel cross-section.

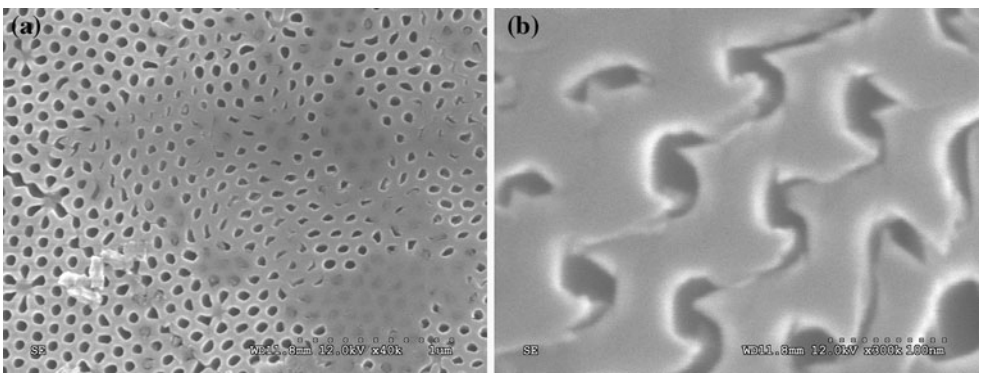

Fig. 14 High magnification SEM image of the corner of a microindentation exhibiting pore crushing (**a**) and nanocrack initiation between pores (**b**) in a crystalline α-alumina membrane

- As-anodized AAO membranes are amorphous, but transform to γ-alumina after heat treatment to 900 °C for 1 h. Nanocrystalline regions of α-alumina begin to form at these temperatures, far below the expected transformation temperature for this phase.
- High temperature heat treatment of AAO to 1200 °C for 1 h results in a stable α-alumina structure as verified by both DSC and TEM analysis. No other phases were observed in the samples after this heat treatment was performed.
- Microhardness testing showed an increase in AAO membrane hardness by a factor of two after transformation from amorphous to crystalline α-alumina.

Acknowledgements Funding for the research was provided by the National Institute of Health (grant NIAID_1R21AI081638-01A2). The authors wish to thank The Loewy Family Foundation for the support through the Loewy Graduate Fellowship (M.K. McQuaig, Jr.), Loewy Visiting Professorship (A. Toro) and Loewy Professorship (W.Z. Misiolek). The authors also thank Adrián Gómez from the National University of Colombia for his valuable help with DSC and TGA measurements.

References

1. Keller F, Hunter MS, Robinson DL (1953) J Electrochem Soc 100:411
2. Masuda H, Fukuda K (1995) Science 268:1466
3. Li XZ, Wei XW, Ye Y (2009) Mater Lett 63:578
4. Sauer G, Brehm G, Schneider S, Nielsch K, Wehrspohn RB, Choi J, Hofmeister H, Gosele U (2002) J Appl Phys 91:3243
5. Masuda H, Satoh M (1995) Jpn J Appl Phys 35:L126
6. Nagaura T, Takeuchi F, Yamauchi Y, Wada K, Inoue S (2008) Electrochem Commun 10:681
7. Thompson GE, Wood GC (1981) Nature 290:230
8. Vrublevsky I, Parkoun V, Schreckenbach J, Marx G (2003) Appl Surf Sci 220:51
9. Ko S, Lee D, Jee S, Park H, Lee K, Hwang W (2006) Thin Solid Films 515:1932
10. Palibroda E, Indrea E (1994) Thin Solid Films 240:88
11. Gall K, Liu Y, Routkevitch D, Finch DS (2006) J Eng Mater Technol 128:225
12. Xia Z, Riester L, Sheldon BW, Curtin WA, Liang J, Yin A, Xu JM (2004) Rev Adv Mater Sci 6:131
13. Sui YC, Cui BZ, Martinez L, Perez R, Sellmyer DJ (2002) Thin Solid Films 406:64
14. Mardilovich PP, Govyadinoy AN, Mukhurov NI, Rzhevskii AM, Paterson R (1995) J Membr Sci 98:131
15. Levin I, Brandon D (1998) J Am Ceram Soc 81:1995
16. Damani RJ, Makroczy P (2000) J Eur Ceram Soc 20:867
17. Dwivedi RK, Gowda G (1985) J Mater Sci Lett 4:331
18. Kirchner A, MacKenzie JD, Brown IWM, Kemmitt T, Bowden ME (2007) J Membr Sci 287:264
19. Mata-Zamora ME, Saniger JM (2005) Rev Mex Fis 51:502
20. Ozao R, Ochiai M, Ichimura N, Takahashi H, Inada T (2000) Thermochim Acta 352–353:91
21. Xiong G, Elam JW, Feng H, Han CY, Wang HH, Iton LE, Curtiss LA, Pellin MJ, Kung M, Kung H, Stair PC (2005) J Phys Chem B 109:14059
22. Kindratenko V (1997) Ph.D. Thesis, University of Antwerp, Belgium, 182 pp
23. Fernandez-Romero L, Montero-Moreno JM, Pellicer E, Peiró F, Cornet A, Morante JR, Sarret M, Müller C (2008) Mater Chem Phys 111:542
24. Lu J, Lu W (2010) In: Proceedings of the 4th international conference on bioinformatics and biomedical engineering (iCBBE), Chengdu, 18–20 June 2010, p 1
25. Le Coz F, Arurault L, Fontorbes S, Vilar V, Datas L, Winterton P (2010) Surf Interface Anal 42:227
26. Sinani AB, Dynkin NK, Lytvinov LA, Konevsky PV, Andreev EP (2009) Bull Russ Acad Sci Phys 73:1380
27. Krell A, Blank P, Ma H, Hutzler T, van Bruggen MPB, Apetz R (2003) J Am Ceram Soc 86:12
28. Ng KY, Lin Y, Ngan AHW (2009) Acta Mater 57:2710
29. Alvey CE, Wood GC (1981) In: Proceedings of the 3rd South African corrosion conference, Pretoria, 17–19 March 1981